Chemical Science

Accepted Manuscript

This article can be cited before page numbers have been issued, to do this please use: J. Chen, Y. Tang, P. Bai and H. Huang, *Chem. Sci.*, 2026, DOI: 10.1039/D6SC03721F.

ROYAL SOCIETY OF CHEMISTRY

rsc.li/chemical-science

View Article Online
DOI: 10.1039/D6SC03721F

Dearomative [2+2] Photocycloaddition to Difluoro Bicyclo[2.1.1]hexane Bioisosteres

Received 00th January 20xx,
Accepted 00th January 20xx

DOI: 10.1039/x0xx00000x

Jun-Jie Chen,[a] Yi-Hui Tang,[a] Pei-Yuan Bai[a] and Huan-Ming Huang* [a,b,c,d]

The development of complex fluorinated bicyclic scaffolds as benzene bioisosteres has emerged as a powerful strategy in drug discovery, yet efficient and general synthetic routes to these structures remain limited. Here, we report a visible-light-driven, energy transfer (EnT)-catalyzed dearomative [2+2] photocycloaddition that converts heteroaromatic-containing *gem*-difluoro alkenes into complex difluorinated bicyclo[2.1.1]hexane bioisosteres. This method operates under mild conditions, exhibits broad heteroaromatic compatibility, and delivers the desired products in good yields with excellent diastereoselectivity. Mechanistic studies are consistent with an energy transfer pathway involving triplet-state diradical intermediates. This work provides a complementary and conceptually new approach to fluorinated bioisosteres that are otherwise difficult to access via classical difluorocarbene insertion or conventional cycloaddition strategies.

Introduction

The replacement of benzene rings with non-aromatic or heteroaromatic bioisosteres has become a powerful strategy in modern drug discovery, offering opportunities to modulate metabolic stability, enhance solubility, and improve target selectivity while preserving the three-dimensional architecture of lead compounds.[1–6] Among these, fluorinated bicyclic scaffolds have emerged as particularly attractive bioisosteres, as the introduction of fluorine can profoundly influence lipophilicity, membrane permeability, and metabolic profiles.[7] Consequently, efficient synthetic methods to access such fluorinated frameworks are in high demand.[8–10]

Classically, difluorocarbene insertion reactions have served as a reliable approach to construct bicyclic systems (**Figure 1A**).[11–16] For example, Ma and co-workers at Merck achieved a selective synthesis of 2,2-difluorobicyclo[1.1.1]pentanes via difluorocarbene insertion into bicyclo[1.1.0]butanes.[11] Mykhailiuk and co-workers developed a practical approach to difluoro-substituted bicyclo[1.1.1]pentanes (2F-BCPs) using a CF_3TMS/NaI system,[12] and further extended this strategy to fluoro-substituted bicyclo[1.1.1]pentanes (F-BCPs) through direct fluorocarbene addition to bicyclo[1.1.0]butanes.[13] However, these methods typically require multi-step syntheses of strained radical precursors such as bicyclo[1.1.0]pentanes or bicyclo[1.1.0]butanes, limiting their overall efficiency and accessibility.[17–25]

More recently, photochemical [2+2] cycloadditions have been exploited for the construction of fluorinated bicyclic scaffolds using various *gem*-difluoro-1,5-dienes as precursors (**Figure 1B**).[26–29] Remarkably, Bi, Hong, and co-workers developed an elegant thermal [2+2] cycloaddition as a route to *gem*-difluoro heterobicyclo[n.1.1]alkanes (**Figure 1C**).[30] Despite these advances, the development of a general, mild, and visible-light-driven method to access complex fluorinated bicyclic bioisosteres directly from readily available heteroaromatic precursors remains an unmet challenge.

Recently, we developed the first example of time-dependent photochemical rearrangements driven by energy transfer (EnT) catalysis[31–40] under visible light conditions, enabled by the introduction of fluorine atoms at the alkene terminus.[41] Inspired by elegant precedents in radical dearomatization[42–44] and our recent work on bioisostere synthesis using radical-polar strategies,[45–47] we hypothesized that replacing a simple aromatic ring with a heteroaromatic ring would enable the synthesis of difluoro bicyclo[2.1.1]hexane bioisosteres through a dearomative [2+2] photocycloaddition.[48–58] Herein, we report the successful realization of this hypothesis (**Figure 1D**). We disclose a visible-light-driven, EnT-catalyzed dearomative [2+2] photocycloaddition that converts heteroaromatic-containing di-fluoro alkenes into complex difluorinated bicyclo[2.1.1]hexane scaffolds in good yields with excellent diastereoselectivity. This method features various heteroaromatic compatibility, mild reaction conditions, and operational simplicity, providing a complementary and conceptually new approach to complex fluorinated bioisosteres that are otherwise difficult to access via classical difluorocarbene insertion or conventional cycloaddition strategies.

---

[a] School of Physical Science and Technology, ShanghaiTech University, Shanghai 201210, China
[b] State Key Laboratory of Fluorine and Nitrogen Chemistry and Advanced Materials, Shanghai Institute of Organic Chemistry, University of Chinese Academy of Sciences, Chinese Academy of Sciences, Shanghai 200032, China
[c] State Key Laboratory of Advanced Medical Materials and Devices, ShanghaiTech University, Shanghai 201210, China
[d] State Key Laboratory of Elemento-Organic Chemistry, Nankai University, Tianjin 300071, China

View Article Online
DOI: 10.1039/D6SC03721F

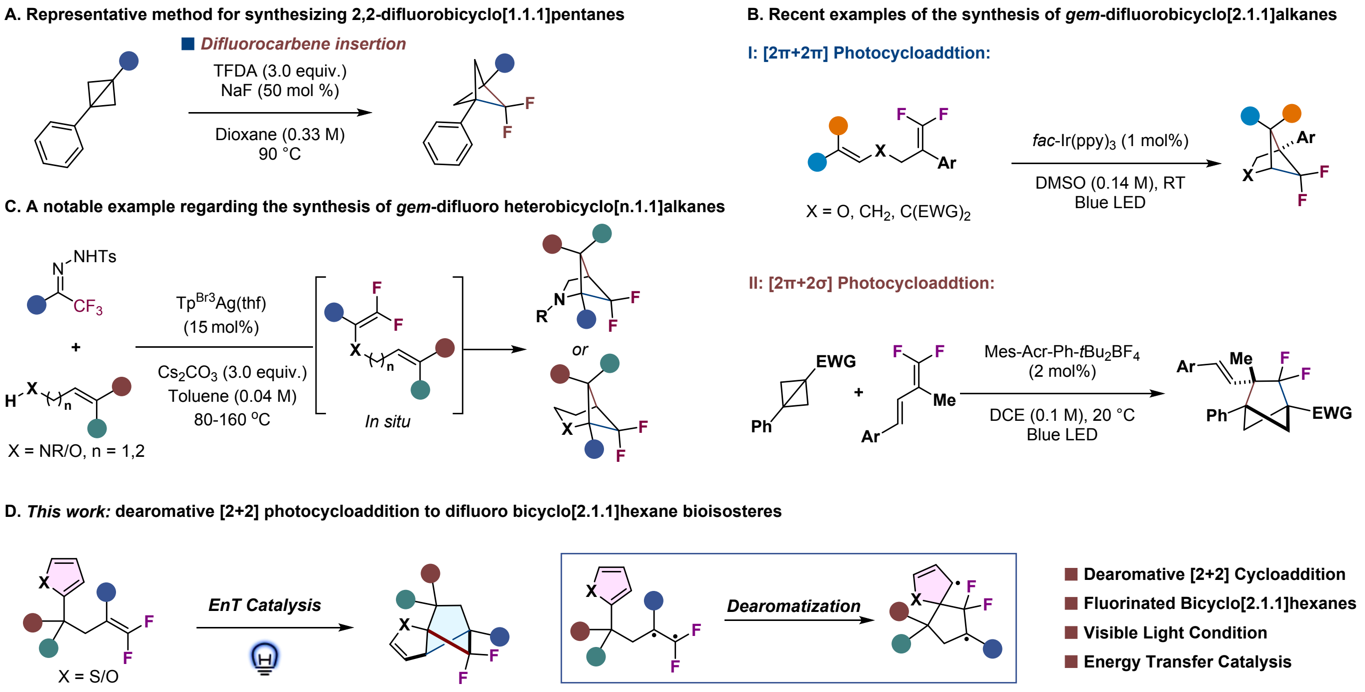

Figure 1. Background and reaction design

Results and Discussion

Reaction design and optimization

Based on our conceptual framework, we efficiently synthesized difluoro-olefin 1a in three steps. Employing 1 mol% of Ir-F as the photocatalyst in acetonitrile under irradiation with the 30 W 450 nm blue LEDs, gem-difluoro-bicyclo[2.1.1]hexane 2 was obtained in 92% isolated yield (Figure 2). Screening of alternative solvents demonstrated that ethyl acetate or dichloromethane derivatives can also afford high yields. However, switching the solvent to *N,N*-dimethylacetamide resulted in a significantly lower yield. Besides, the Ir-Me also worked well and provided a useful alternative to Ir-F. In contrast, replacing Ir-F with other common organic photocatalysts—such as Benzophenone, Thioxanthone or 4CzIPN resulted in only moderate yields of the desired product. Control experiments confirmed that no product formation occurred in the absence of light, ruling out a thermal process. Omitting the photocatalyst resulted in low product yields, indicating that **1a** can be directly excited at 365 nm.

View Article Online
DOI: 10.1039/D6SC03721F

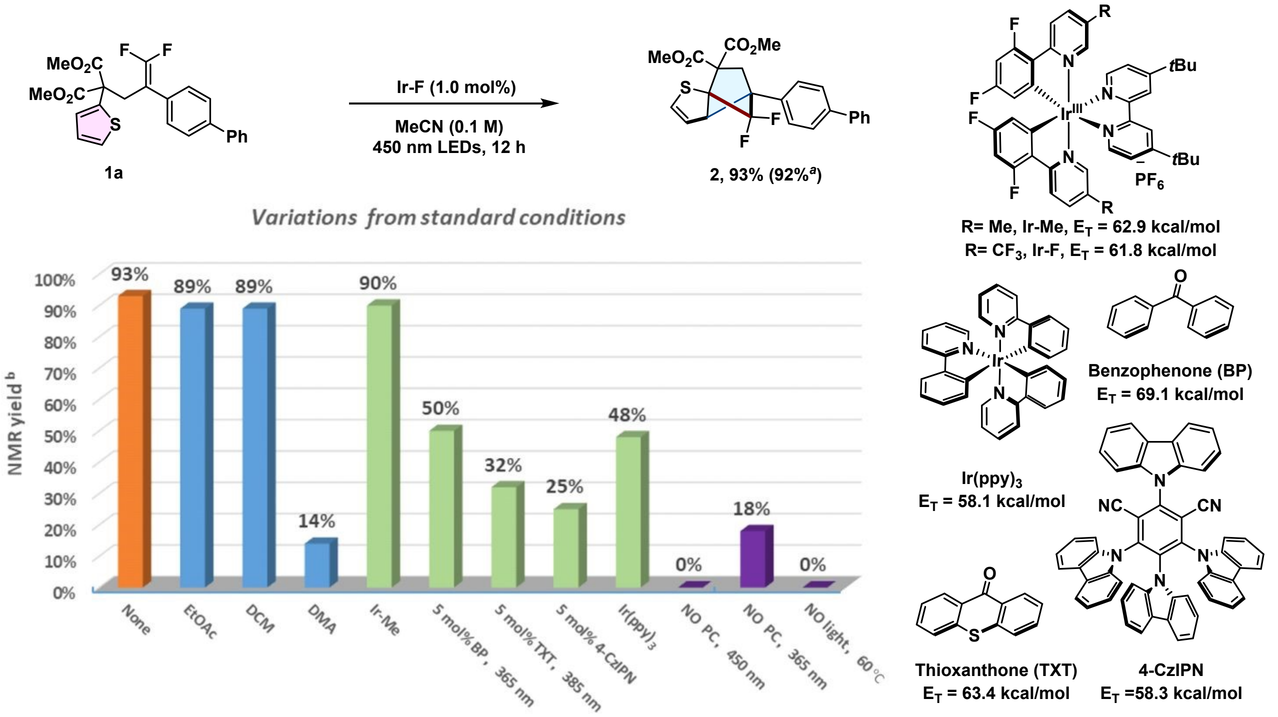

Figure 2. Reaction Design and Optimization. Standard condition: **1a** (0.2 mmol, 1 equiv.), Ir-F (1 mol%), and MeCN (0.1 M) at room temperature under 30 W 450 nm LEDs with a cooling system for 12 h under N_2. ^{a} Isolated yield. ^{b} ^{1}H NMR yield (CH_2Br_2 as an internal standard).

Substrate scope

Having secured the initial outcomes, we undertook a systematic investigation into the substrate scope (**Figure 3**). Pleasingly, a range of functional groups including methyl (**4**), *tert*-butyl (**5**), bromide (**6**), fluoro (**7**), chloride (**8, 9**), methoxyl (**12**), trifluoromethoxyl (**13**) and naphthyl (**16, 17**) were all well tolerated, affording good to high isolated yields. The stereochemistry of the major isomer of **17** was confirmed by X-ray analysis (**CCDC 2541039**). The method also demonstrated tolerance to heterocycles, including benzothiophene (**18**), quinoline (**19**), dibenzofuran (**20**) and dibenzothiophene (**21**). Furthermore, the substrate scope was further extended to include compounds with diene (**22**) and alkyne motifs (**23–25**). These proved to be well-tolerated under the standard conditions, and the desired products were successfully obtained in good to excellent isolated yields. Finally, we screened several complex substrates containing natural product motifs (**26-33**), which successfully yielded the target products in 71% to 85% isolated yields, underscoring the potential for late-stage functionalization.

The reaction was also applicable to substrate **34**, which bears two hydrogen atoms, albeit affording a lower isolated yield of 40% (**Figure 4**). Notably, substrates incorporating both a methyl and an ester group (**1ah** and **1ai**) were well-tolerated, delivering the desired products **35** and **36** in excellent isolated yields of 81–87%. Subsequently, we will shift our focus to studying the various functional groups attached to thiophene motifs. The reaction demonstrated broad compatibility with alkyl (**38- 40**), ester (**41**) and phenyl (**42-44**) groups, and also tolerated a dimethyl-substituted thiophene ring (**45**), generally providing the desired products in good to high yields. Other heterocyclic systems, including furan (**46**), 3-thiophene (**47**) benzothiophene (**48**) and benzofuran (**49**), also proved amenable to this dearomatization protocol. Unfortunately, the indole motif was also explored, the desired product (**50**) could not be formed successfully.

When we attempted to use olefins lacking the difluoro group (**1ax**), a significant decrease in reaction yield was observed (**51**). This result indicates that difluoroalkenes are very important in

View Article Online
DOI: 10.1039/D5SC07721F

our structure. We speculate that it may be due to the interaction between the C–F σ* orbital and the SOMO orbital which lowers the energy barrier for diradical generation and facilitates the reaction. However, the use of olefins bearing dichloro groups (**1ay**) or a methyl group (**1az**) resulted in poor reaction efficiency.

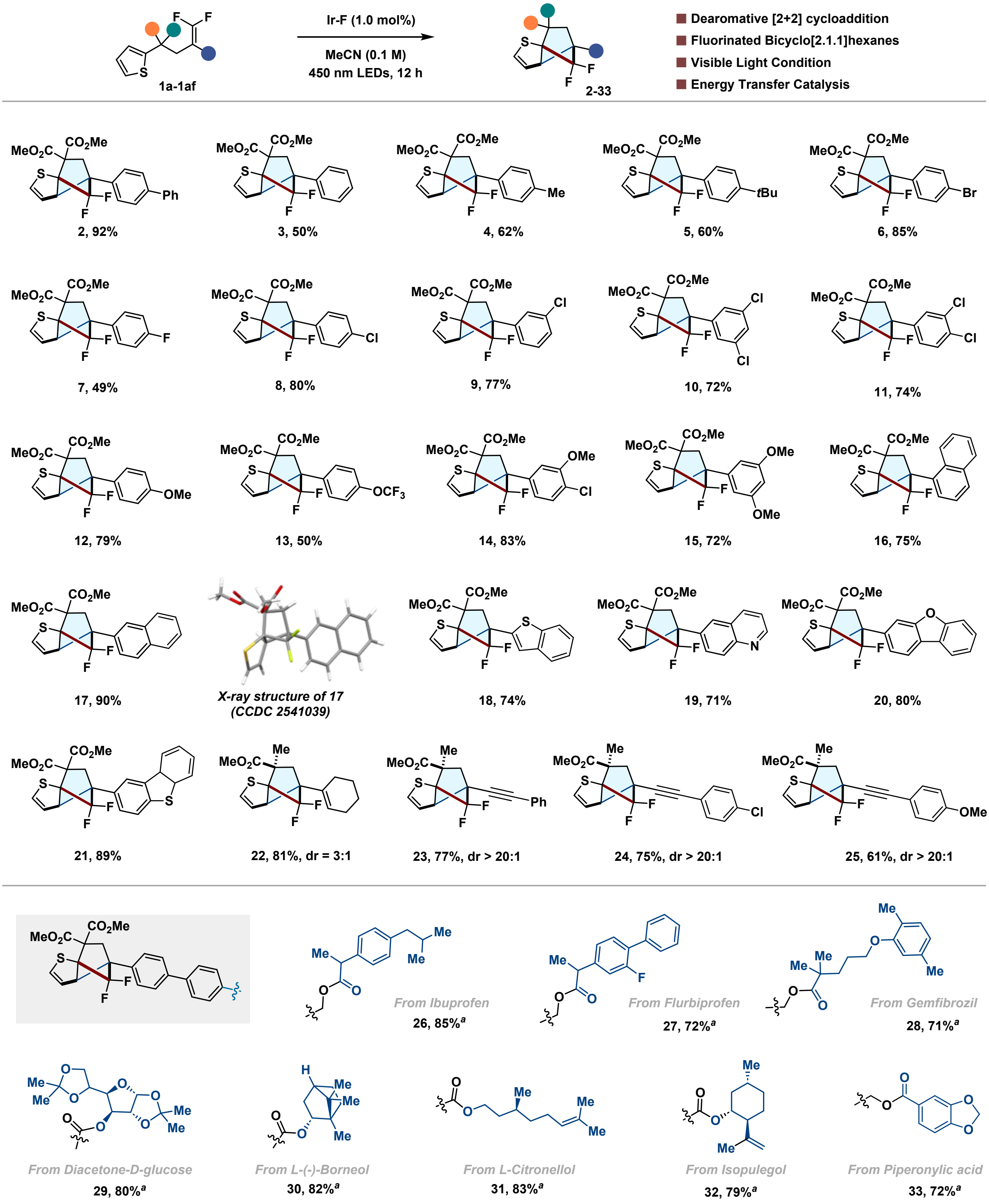

View Article Online
DOI: 10.1039/D6SC03721F

Figure 3. Substrate scope to construct fluorinated bicyclo[2.1.1]hexanes. Reaction condition: **1a-1af** (0.2 mmol, 1 equiv.), Ir-F (1.0 mol%) and MeCN (2.0 mL, 0.1 M) at room temperature under 30 W 450 nm LEDs with a cooling system for 12 h under N_2. ^{a} Using MeCN (3.0 mL, 0.067 M) as solvent.

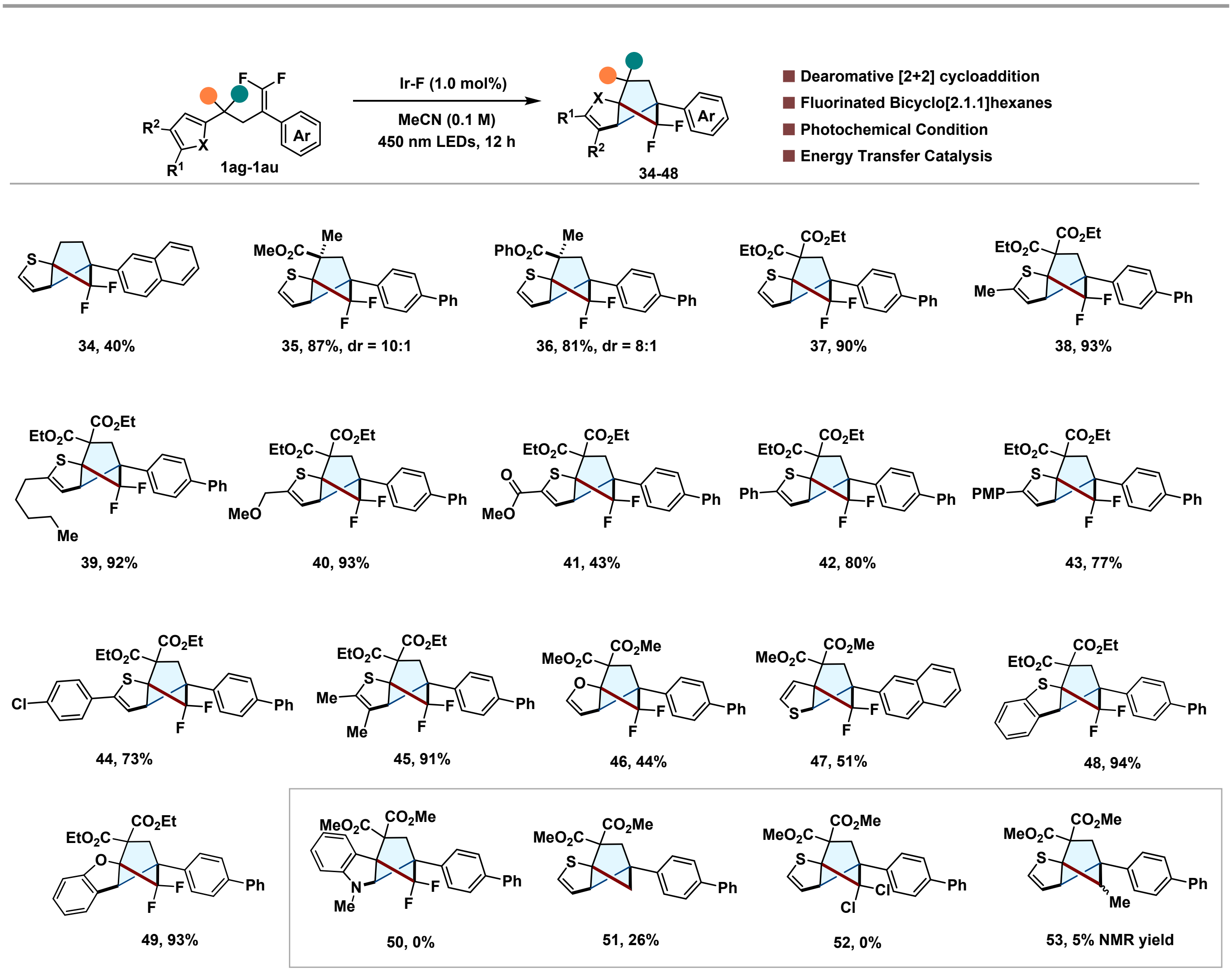

Figure 4. Substrate scope with various heteroaromatic rings. Reaction condition: **1ag-1az** (0.2 mmol, 1 equiv.), Ir-F (1.0 mol%) and MeCN (2.0 mL, 0.1 M) at room temperature under 30 W 450 nm LEDs with a cooling system for 12 h under N_2.

Synthetic application and mechanistic studies

To further investigate the robustness of this mild protocol, we first performed gram-scale reactions using substrate **1a**. Under the optimized conditions, an isolated yield of 88% was achieved at a 3.5 mmol scale (**Figure 5A**). Additionally, the reaction was successfully implemented in a continuous-flow photo-reactor, which significantly shortened the reaction time (t_R = 180 min) and delivered product **6** in 75% isolated yield at the gram-scale level (**Figure 5B**). Notably, product **6** could be efficiently transformed into various functionalized products (**Figure 5C**) through Suzuki coupling (**54**), reduction followed by Nucleophilic substitution (**55**), Sonogashira coupling (**56**), and hydrogenation (**57**). Furthermore, radical inhibition and triplet state quenching experiments were conducted. In these studies, the formation of product **2** was substantially suppressed, demonstrating that radical species are involved in the catalytic system and suggesting that the protocol may proceed via an energy transfer mechanism (**Figure 5D**). UV/Vis experiments confirmed that only the photocatalyst absorbs visible light

(**Figure 5E**); fluorescence studies (**Figure 5F**) and Stern–Volmer quenching experiments (**Figure 5G**) revealed that substrate **1a** effectively quenches the photoexcited photocatalyst. Moreover, the measured quantum yield (φ = 0.045) suggests the reaction unlikely proceeds via a radical chain mechanism. Based on these mechanistic investigations, we propose that the key diradical species **1a*** efficiently is generated via an energy transfer mechanism under visible light conditions, which subsequently undergoes dearomatization to form intermediate **I**, followed by intersystem crossing (ISC), to afford the diradical intermediate **II**, which ultimately participates in radical coupling to yield the final product **2** (**Figure 5H**).

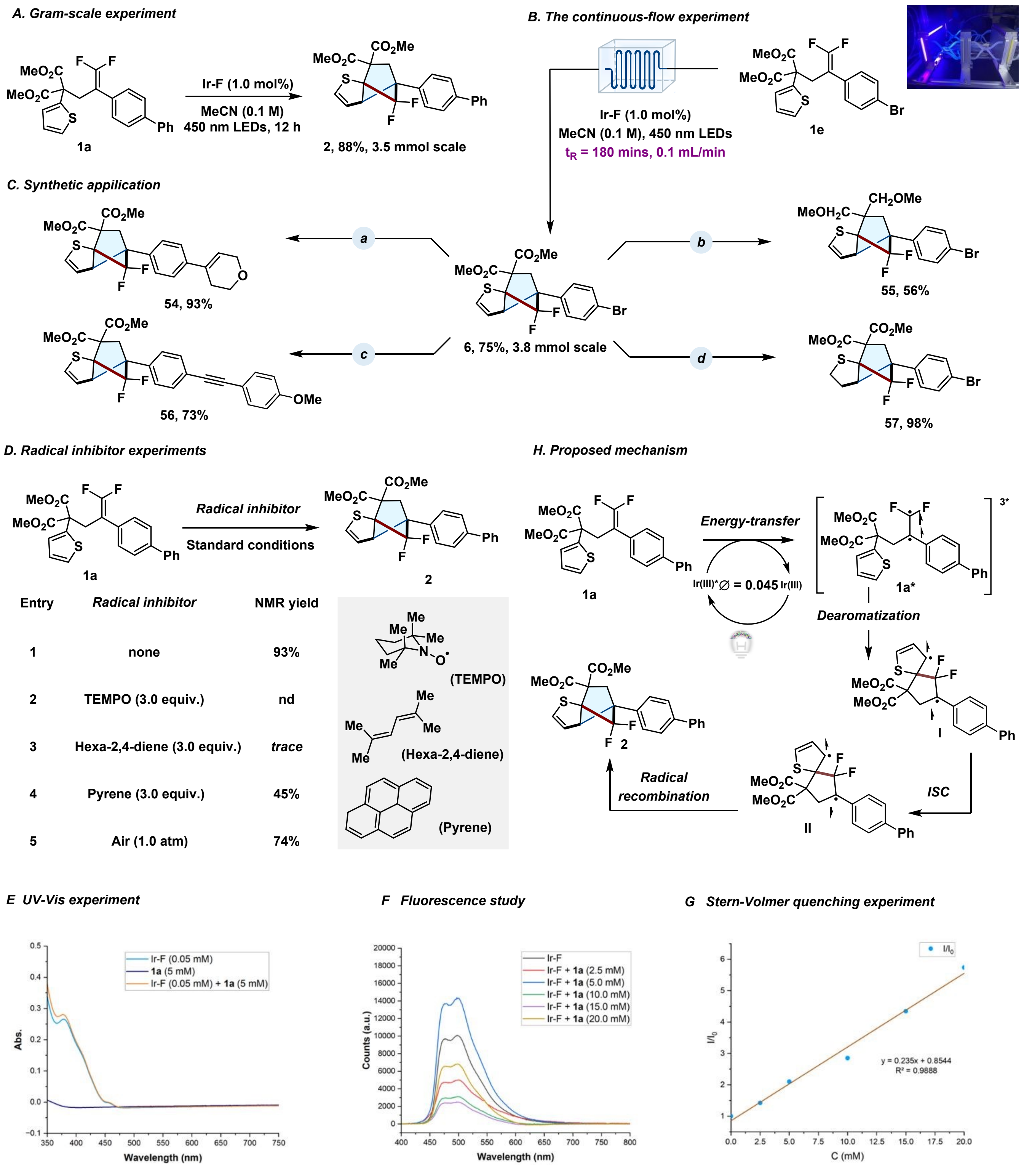

Entry	Radical inhibitor	NMR yield
1	none	93%
2	TEMPO (3.0 equiv.)	nd
3	Hexa-2,4-diene (3.0 equiv.)	*trace*
4	Pyrene (3.0 equiv.)	45%
5	Air (1.0 atm)	74%

View Article Online
DOI: 10.1039/D6SC03721F

Figure 5. Synthetic transformations and mechanistic studies. [a] 3,6-dihydro-2*H*-pyran-4-boronic acid pinacol ester (1.5 equiv.), Pd(PPh$_3$)$_4$ (5.0 mol%), K$_2$CO$_3$ (2.0 equiv.), THF/H$_2$O (v/v = 3/1, 0.1 M), 60 °C, overnight; [b] 1) LiAlH$_4$ (3.0 equiv.), THF (0.1 M), 0 °C to RT; 2) NaH (3.0 equiv.), THF (0.1 M) then MeI (3.0 equiv.); [c] Pd(PPh$_2$)Cl$_2$ (5.0 mol%), 4-ethynylanisole (1.5 equiv.), CuI (10.0 mol%), Et$_3$N (0.1 M), 60 °C, overnight; [d] Pd/C (10 mol%), H$_2$ (1 atm), MeOH (0.1 M), RT, 12 h.

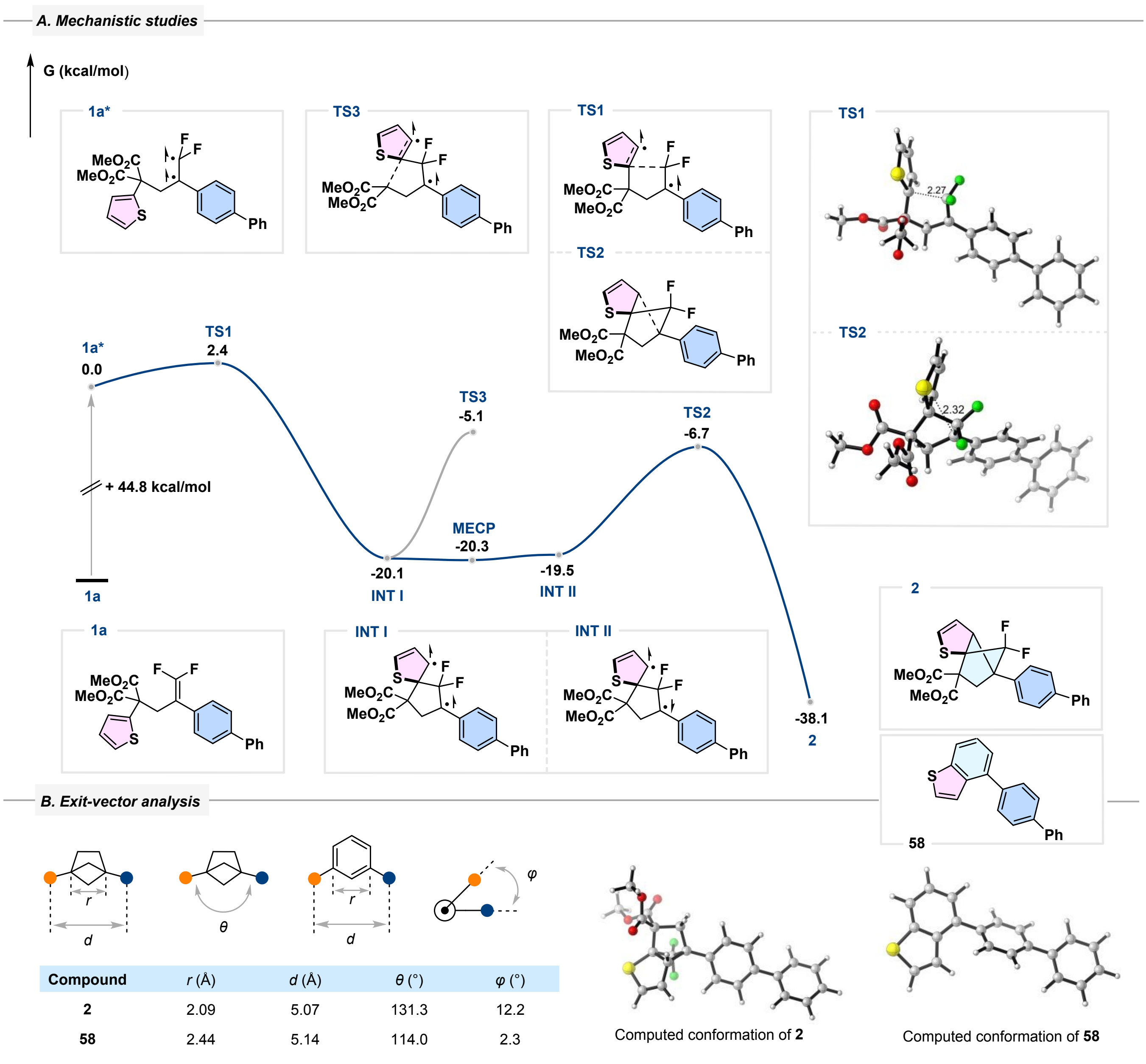

Compound	*r* (Å)	*d* (Å)	*θ* (°)	*φ* (°)
2	2.09	5.07	131.3	12.2
58	2.44	5.14	114.0	2.3

Figure 6. Computational studies of dearomative [2+2] photocycloaddition to difluoro bicyclo[2.1.1]hexane bioisosteres. A. Gibbs free energy profile for the reaction pathway. **B.** Exit-vector analysis.

Computational studies

To corroborate the experimental observations and elucidate the detailed energy landscape, density functional theory (DFT) calculations were conducted for substrate **1a** at the SMD(MeCN)/ωB97X-D/Def2-TZVPP//ωB97X-D/Def2-SVP level (see the Supporting Information for details). The computed Gibbs free energy profile (**Figure 6A**) reveals that the excitation of **1a** to its first triplet state (**1a***) requires 44.8 kcal/mol. For convenience, **1a*** was taken as the zero point on the potential energy surface. The reaction is initiated by energy transfer, which promotes substrate **1a** to its triplet state **1a***. Subsequently, **1a*** undergoes 5-*exo*-trig cyclization via **TS1** with a low energy barrier of 2.4 kcal/mol, leading to spirocyclic diradical species **INT I** (-20.1 kcal/mol). This intermediate then undergoes the intersystem crossing (ISC) via a minimum energy crossing point (MECP, -20.3 kcal/mol) to give open-shell singlet diradical species **INT II** (−19.5 kcal/mol). Owing to the spirocyclic structure, the intramolecular coupling is not readily feasible.

View Article Online
DOI: 10.1039/D6SC03721F

Nevertheless, thermodynamically driven by the formation of a stable product, **INT II** overcomes a barrier of 12.8 kcal/mol via **TS2** to form the C–C bond, yielding the final product **2** (-38.1 kcal/mol), thereby completing the construction of the difluoro bicyclo[2.1.1] framework within the molecule. An alternative reaction pathway involves β-scission of **INT I** via **TS3** (-5.1 kcal/mol) to achieve rearomatization, followed by ISC and radical coupling to afford the thiophene ring-migration product. However, the β-scission step is associated with a relatively high activation barrier ($\Delta G^{\ddagger}$ = 15.0 kcal/mol), rendering this pathway less favorable. Consistent with the computational prediction, such a product was not observed experimentally.

To evaluate the structural relevance of difluorinated bicyclo[2.1.1]hexane (BCHs) **2** and its aromatic counterparts **58** , we performed an exit-vector analysis (**Figure 6B**). The relative spatial arrangement of the vectors is described by four geometric parameters: the distance between carbon atoms (*r*), the distance between two substituents (*d*), the dihedral angle (*φ*), and the angle (*ϑ*), which is the angle between the two vectors pointing outward from the ring along the two covalent bonds. For difluorinated BCHs **2**, computational evaluation revealed that the parameters *r*, *d* and *φ* are closely comparable. However, the angle (*ϑ*) is 17◦ larger than that observed in meta-benzene. This comparison is skewed by the benzo[b]thiophene-induced angular contraction in **58** (*ϑ* = 114.0°). These data serve as compelling evidence corroborating difluorinated BCHs **2** as a bioisostere of the benzene ring.

Conclusions

In summary, we have developed a visible-light-driven, energy transfer-catalyzed dearomative [2+2] photocycloaddition that converts readily available heteroaromatic-containing *gem*-difluoro alkenes into complex difluorinated bicyclo[2.1.1]hexane scaffolds. This method operates under mild conditions, exhibits broad functional-group tolerance—including compatibility with various heteroarenes and natural-product-derived motifs—and delivers the desired products in good to excellent yields with exceptional diastereoselectivity. Mechanistic and computational studies support an energy-transfer pathway involving triplet-state diradical intermediates. The resulting fluorinated bicyclic frameworks serve as promising bioisosteres of benzene rings, offering opportunities to modulate physicochemical properties in drug discovery. More broadly, this work establishes a conceptually new paradigm for constructing fluorinated three-dimensional architectures from planar aromatic precursors, paving the way for further innovations in bioisostere design and photochemical synthesis.

Author contributions

H.-M. H. conceived and directed the research; J.-J. C. and P.-Y. B. performed the experiments and analyzed the data. Y.-H. T. performed the DFT calculation and drafted the computation section. H.-M. H. wrote the manuscript with contributions from all authors.

Conflicts of interest

There are no conflicts to declare.

Data availability statements

All data supporting the findings including the experimental procedures, characterization of compounds and computational data are available within the article and its Supporting Information.

Acknowledgements

We are grateful for financial support from the National Natural Science Foundation of China (22471168 to H.-M. H.), the State Key Laboratory of Fluorine and Nitrogen Chemistry and Advanced Materials (2026PT0007), the State Key Laboratory of Elemento-organic Chemistry and the startup funding from ShanghaiTech University (H.-M. H.). We thank the HPC Platform of ShanghaiTech University for computing time and Kai-Dian Li (ShanghaiTech University) for help with X-ray analysis.

Notes and references

1 F. Lovering, J. Bikker and C. Humblet, *J. Med. Chem.*, 2009, **52**, 6752–6756.
2 P. K. Mykhailiuk, *Org. Biomol. Chem.*, 2019, **17**, 2839–2849.
3 J. Tsien, C. Hu, R. R. Merchant and T. Qin, *Nat. Rev. Chem.*, 2024, **8**, 605–627.
4 J. M. Anderson, N. D. Measom, J. A. Murphy and D. L. Poole, *Angew. Chem. Int. Ed.*, 2021, **60**, 24754–24769.
5 P. Bellotti and F. Glorius, *J. Am. Chem. Soc.*, 2023, **145**, 20716–20732.
6 S. Cuadros, J. Paut, E. Anselmi, G. Dagousset, E. Magnier and L. Dell'Amico, *Angew. Chem. Int. Ed.*, 2024, **63**, e202317333.
7 K. Müller, C. Faeh and F. Diederich, *Science*, 2007, **317**, 1881–1886.
8 W. K. Hagmann, *J. Med. Chem.*, 2008, **51**, 4359–4369.
9 N. A. Meanwell, *J. Med. Chem.*, 2018, **61**, 5822–5880.
10 C. Ni and J. Hu, *Chem. Soc. Rev.*, 2016, **45**, 5441–5454.
11 X. Ma, D. L. Sloman, Y. Han and D. J. Bennett, *Org. Lett.*, 2019, **21**, 7199–7203.
12 R. M. Bychek, V. Hutskalova, Y. P. Bas, O. A. Zaporozhets, S. Zozulya, V. V. Levterov and P. K. Mykhailiuk, *J. Org. Chem.*, 2019, **84**, 15106–15117.
13 R. Bychek and P. K. Mykhailiuk, *Angew. Chem. Int. Ed.*, 2022, **61**, e202205103.
14 X. Ma, W. Pinto, L. N. Pham, D. L. Sloman and Y. Han, *Eur. J. Org. Chem.*, 2020, **2020**, 4581–4605.
15 Z. Zhu, J. Tang, M. Coe, A. Knieb, Y. Xu, D. Lin, C. Zhang and G. K. Surya Prakash, *Adv. Synth. Catal.*, 2025, **367**, e202401475.
16 J. C. Sharland and H. M. L. Davies, *Org. Lett.*, 2023, **25**, 5214–5219.
17 X. Yang, J. Wang, Y. Xiao and J. Feng, *Angew. Chem. Int. Ed.*, 2025, e202505803.
18 Y. Xiao, L. Tang, X.-C. Yang, N.-Y. Wang, J. Zhang, W.-P. Deng and J.-J. Feng, *CCS Chem.*, 2025, **7**, 1903–1934.
19 F.-S. He, S. Xie, Y. Yao and J. Wu, *Chine. Chem. Lett.*, 2020, **31**, 3065–3072.
20 S. Deswal, R. Chandra Das and A. T. Biju, *Chem. Soc. Rev.*, 2026, **55**, 5572-5589
21 A. Fawcett, *Pure Appl. Chem.*, 2020, **92**, 751–765.
22 J. Turkowska, J. Durka and D. Gryko, *Chem. Commun.*, 2020, **56**, 5718–5734.
23 M. Golfmann and J. C. L. Walker, *Commun. Chem.*, 2023, **6**, 9.

View Article Online
DOI: 10.1039/D6SC03721F

24 24 C. B. Kelly, J. A. Milligan, L. J. Tilley and T. M. Sodano, *Chem. Sci.*, 2022, **13**, 11721–11737.

25 R. I. Revie, J. Ragus and E. A. Anderson, *Chem. Soc. Rev.*, 2026, **55**, 941–954.

26 W. Zeng, M. Li, S. Wu, A. Abdukade and L. Zhou, *Org. Chem. Front.*, 2024, **11**, 3421–3426.

27 M. Wu, K. Ren, C. Zou, J. Chen, R. Ma, C. Zhu and C. Feng, *Chin. Chem. Lett.*, 2025, **36**, 110213.

28 Z. Fu, J. Cheng, X.-X. Li, X. Li and S. Yu, *Org. Lett.*, 2024, **26**, 9961–9966.

29 M. Wu, J. Wang, S. Wang, C. Zhu, J. Zhang and C. Feng, *Org. Lett.*, 2025, **27**, 10235–10240.

30 Y. Ning, R. Wu, Y. Ning, Q. Song, J. Deng, Q. Jiao, P. Sivaguru, J. Mlynarski, G. de Ruiter, X. Hong and X. Bi, *Nat. Chem.*, 2026, **18**, 283–293.

31 F. Strieth-Kalthoff, M. J. James, M. Teders, L. Pitzer and F. Glorius, *Chem. Soc. Rev.*, 2018, **47**, 7190–7202.

32 Q. Zhou, Y. Zou, L. Lu and W. Xiao, *Angew. Chemie Int. Ed.*, 2019, **58**, 1586–1604.

33 F. Strieth-Kalthoff and F. Glorius, *Chem*, 2020, **6**, 1888–1903.

34 J. Großkopf, T. Kratz, T. Rigotti and T. Bach, *Chem. Rev.*, 2022, **122**, 1626–1653.

35 M. Zhu, X. Zhang, C. Zheng and S.-L. You, *Acc. Chem. Res.*, 2022, **55**, 2510–2525.

36 T. Neveselý, M. Wienhold, J. J. Molloy and R. Gilmour, *Chem. Rev.*, 2022, **122**, 2650–2694.

37 S. Dutta, J. E. Erchinger, F. Strieth-Kalthoff, R. Kleinmans and F. Glorius, *Chem. Soc. Rev.*, 2024, **53**, 1068–1089.

38 Q. Dong, Y. Ke, Y. Zhang and H. Huang, *Angew. Chem. Int. Ed.*, 2025, **64**, e202519769.

39 K. L. Skubi, T. R. Blum and T. P. Yoon, *Chem. Rev.*, 2016, **116**, 10035–10074.

40 J.-J. Chen, S. Chen, Q. Wang and H. Huang, *Chem. Soc. Rev.*, 2026, **55**, 6221–6256.

41 S. Wen, Y. Zhang, J. Chen, X. Xue and H. Huang, *Angew. Chem. Int. Ed.*, 2025, **64**, e202516222.

42 Y.-Z. Cheng, Z. Feng, X. Zhang and S.-L. You, *Chem. Soc. Rev.*, 2022, **51**, 2145–2170.

43 M. Li, Y.-Z. Cheng and S.-L. You, *Sci. Adv.*, 2026, **12**, eaed5284.

44 J. Chen, W. Zhang, D. Huang, J. Wu and X. Wu, *Asian J. Org. Chem.*, 2025, **14**, e00382.

45 S.-Y. Tang, Z.-J. Wang, J.-J. Wu, Z.-X. Xing, Z.-Y. Du and H.-M. Huang, *Chem. Sci.*, 2025, **16**, 11908–11917.

46 Y. Zhang, K.-D. Li, S. Yu, K. Pan, H. Xu and H.-M. Huang, *J. Am. Chem. Soc.*, 2025, **147**, 33700–33710.

47 H. Ran, Y. Zheng and H. Huang, *Angew. Chem. Int. Ed.*, 2026, DOI:10.1002/anie.6606811.

48 M. D. Kärkäs, J. A. Porco and C. R. J. Stephenson, *Chem. Rev.*, 2016, **116**, 9683–9747.

49 S. Poplata, A. Tröster, Y.-Q. Zou and T. Bach, *Chem. Rev.*, 2016, **116**, 9748–9815.

50 Y. Zhang, Y. Guo, Y. Zhang, S. Liu and X. Shen, *Chem Catal.*, 2025, **5**, 101200.

51 N. Hu, H. Jung, Y. Zheng, J. Lee, L. Zhang, Z. Ullah, X. Xie, K. Harms, M. Baik and E. Meggers, *Angew. Chem. Int. Ed.*, 2018, **130**, 6350–6354.

52 M. J. James, J. L. Schwarz, F. Strieth-Kalthoff, B. Wibbeling and F. Glorius, *J. Am. Chem. Soc.*, 2018, **140**, 8624–8628.

53 S. Stegbauer, C. Jandl and T. Bach, *Angew. Chemie Int. Ed.*, 2018, **57**, 14593–14596.

54 J. Ma, F. Schäfers, C. Daniliuc, K. Bergander, C. A. Strassert and F. Glorius, *Angew. Chem. Int. Ed.*, 2020, **59**, 9639–9645.

55 M. S. Oderinde, E. Mao, A. Ramirez, J. Pawluczyk, C. Jorge, L. A. M. Cornelius, J. Kempson, M. Vetrichelvan, M. Pitchai, A. Gupta, A. K. Gupta, N. A. Meanwell, A. Mathur and T. G. M. Dhar, *J. Am. Chem. Soc.*, 2020, **142**, 3094–3103.

56 M. S. Oderinde, S. Jin, T. G. M. Dhar, N. A. Meanwell, A. Mathur and J. Kempson, *Tetrahedron*, 2022, **103**, 132087.

57 E. R. Sauvé, D. M. Mayder, S. Kamal, M. S. Oderinde and Z. M. Hudson, *Chem. Sci.*, 2022, **13**, 2296–2302.

58 J. Wang, Q. Fu, S. Cao, X. Lv, Y. Yin, X. Ban, X. Zhao and Z. Jiang, *J. Am. Chem. Soc.*, 2024, **146**, 22840–22849.

View Article Online
DOI: 10.1039/D6SC03721F

Data availability statements

All data supporting the findings including the experimental procedures, characterization of compounds and computational data are available within the article and its Supporting Information.